Subsolidus Phase Equilibria of Fe-Ni-X-O (X = Mg, Al) Systems in Air

M.A. RHAMDHANI, T. HIDAYAT, P.C. HAYES, and E. JAK

The phase equilibria of Fe-Ni-X-O (X = Mg, Al) systems, including their lower-order systems, at temperatures between 1200 °C and 1600 °C in air in the subsolidus region, have been experimentally studied. In the present study, the 'Fe_2O_3'-MgO, 'Fe_2O_3'-Al_2O_3, and NiO-Al_2O_3 binary phase diagrams, as well as the ternary phase diagrams in the Fe-Ni-Mg-O and Fe-Ni-Al-O systems projected onto the Fe-Mg-Ni and Fe-Al-Ni planes, have been constructed. Differences have been found between the present measurements, the previously published data, and the FactSage predictions, especially in the lower-order systems. It is suggested that the improved experimental techniques used in the present study, which involve carefully planned equilibration procedures followed by electron probe X-ray microanalyses (EPMA), provide more accurate and precise measurements of the phase boundaries and phase compositions.

DOI: 10.1007/s11663-008-9213-z

I. INTRODUCTION

In the Caron process,[1] nickel is extracted from nickel laterite through a combination of pyrometallurgy and hydrometallurgy processes. The nickel laterite, a mixture of limonitic (oxides/hydroxides) and saprolitic (silicates/hydrosilicates) ores, is processed through reduction roasting prior to leaching in an ammoniacal solution. The reduction roasting is carried out at an average reactor temperature of 750 °C. The nickel laterite, however, can be exposed to a temperature in excess of 1200 °C in the area close to the burner. The pregnant liquor resulting from the leaching process is then purified and precipitated to form an intermediate product, basic nickel carbonate (BNC). The BNC is further reduced, to produce nickel metal product.[2]

Detailed thermodynamic information on the phase equilibria in the Fe-Ni-X-O and Fe-Ni-X-Si-O (X = Mg, Al, Cr) systems, including information on the nickel distribution between the phases present, is vital for the control of the reduction roasting process and to achieve maximum nickel extraction. It has been shown previously[3,4] that the optimum conditions, from the thermodynamic point of view (*e.g.*, temperature and effective oxygen partial pressure), are different for the processing of limonitic and saprolitic laterite ores.

Previous experimental studies[5] on the phase equilibria of the Fe-Ni-O system in air and at various oxygen partial pressures have provided the basis for the present study. In the present article, the phase equilibria of the Fe-Ni-X-O (X = Mg, Al) system in air between the temperatures 1200 °C and 1600 °C in the subsolidus regions are investigated using improved experimental techniques, which include equilibration and quenching followed by electron probe X-ray microanalysis (EPMA) examination.

A number of studies have been undertaken on the phase equilibria of the Fe-Ni-O[5–23] system. The most recent study on this system was carried out at temperatures between 800 °C and 1600 °C, in air and at oxygen partial pressures (pO_2) between $10^{-11.8}$ and 1 atm, using the equilibration and quenching techniques and followed by EPMA.[5] The solubility of iron in bunsenite (Ni,Fe)O at 1200 °C is reported to be 16.1 Fe mole pct in air and increases up to a maximum of 66.2 Fe mole pct with a decreasing oxygen partial pressure down to $pO_2 = 10^{-8.3}$ atm. The solubility of iron in bunsenite is also reported to increase with increasing temperature. The solubility of iron at 1200 °C in a Ni,Fe alloy is reported to increase with decreasing pO_2, while the solubility of nickel in wustite (Fe,Ni)O decreases with decreasing pO_2.

Several studies on the phase equilibria of the Fe-Mg-O system have been carried out.[24–30] The most recent study of the subsolidus phase equilibria in the Fe-Mg-O system was carried out by Hansson *et al.*[30] at 1200 °C to 1600 °C; the focus of the study was to define the extent of the spinel $(Fe,Mg)_3O_{4+y}$ and periclase (Mg,Fe)O solid solutions. Hansson *et al.* used the equilibration-quenching techniques and EPMA in this study; they reported that the concentration of iron in the spinel in equilibrium with periclase increases with increasing temperature. The abnormal inflection in the spinel composition at the spinel/periclase boundary at approximately 1400 °C reported by Wilshee and White[29] was not observed in their study.

Muan[31,32] carried out a study to investigate the occurrence of the $Fe_2O_3{\cdot}Al_2O_3$ phase in the

M.A. RHAMDHANI, formerly Postdoctoral Research Fellow, with the Pyrometallurgy Research Centre, School of Engineering, The University of Queensland, is Lecturer, Faculty of Engineering and Industrial Sciences, Swinburne University of Technology, Hawthorn, VIC 3122, Australia. Contact e-mail: arhamdhani@swin.edu.au T. HIDAYAT, Postgraduate Student, P.C. HAYES and E. JAK, Professors, are with the Pyrometallurgy Research Centre, School of Engineering, The University of Queensland, Brisbane, QLD 4072, Australia.

Manuscript submitted September 2, 2008.
Article published online January 14, 2009.

'Fe_2O_3'-Al_2O_3 system in air and at a 1-atm O_2 pressure, using high-temperature equilibration and quenching techniques. The phase identification in the equilibrated samples was carried out using optical microscopy and the X-ray diffraction (XRD) method (measurements of the *d*-spacings of the crystalline phases). The $Fe_2O_3 \cdot Al_2O_3$ was reported to exist in stable equilibrium at subsolidus temperatures between 1318 °C and 1410 °C. It is indicated in the article that, in the subsolidus region (*e.g.*, below 1340 °C), an equilibrium condition was difficult to be achieved in a reasonable time. At temperatures above 1340 °C, equilibrium was achieved in 1 to 3 days. The most recent work on the 'Fe_2O_3'-Al_2O_3 system was carried out by Hansson *et al.*[33] as part of the study on the phase equilibria of the Al-Fe-Zn-O system in air. Hansson *et al.* also used the equilibration and quenching techniques; however the phase identification and phase boundaries were determined by direct measurement of phase compositions using EPMA. Hansson *et al.* reported a significantly higher solubility of Al_2O_3 in hematite $(Fe,Al)_2O_3$ at 1250 °C compared to the results from Muan and Gee.[31] The maximum solubility of Al_2O_3 in the $Al_2O_3 \cdot Fe_2O_3$ phase was also reported to be 0.03 mole fraction Al_2O_3, larger than reported by Muan and Gee.

Phillips *et al.*[34] conducted a study on the phase equilibria of the NiO-Al_2O_3-SiO_2 system that also includes some work on the NiO-Al_2O_3 phase equilibria. High-temperature equilibration and quenching techniques were used in the study. The phase identification was carried out using petrographic microscopy and XRD analysis. In the subsolidus region, the following phases were reported to present: NiO solid solution, $NiO \cdot Al_2O_3$ spinel, and corundum Al_2O_3. At 1650 °C, the $NiO \cdot Al_2O_3$ spinel phase was observed in a composition range of approximately 38 to 50 mole pct Al_2O_3. Due to problems with NiO loss at high temperature and the limitations of the XRD technique for phase identification, accurate phase boundaries could not be obtained by Phillips *et al.*[34] The NiO solid solution field in the NiO-Al_2O_3 binary phase diagram constructed in the work by Phillips *et al.* was based on previously reported data.[35]

No experimental work has been found in the literature on the phase equilibria of the Fe-Ni-Mg-O and Fe-Ni-Al-O systems.

II. EXPERIMENTAL DESIGN

A. *Experimental Techniques*

The phase equilibria of the Fe-Ni-O-Mg and Fe-Ni-O-Al systems were investigated using the equilibration and quenching techniques, followed by measurements of phase compositions using the EPMA technique. These improved techniques, which have a number of advantages, including enhanced accuracy and reliability,[36] were developed and have been used extensively by the authors for studying the phase equilibria of oxides. The use of EPMA following equilibration makes it possible to determine whether all phases have reached steady-state composition and equilibrium has been achieved. The techniques are described briefly in the following paragraphs.

B. *Sample preparation*

The following oxide and metal powders, obtained from Sigma-Aldrich (Sydney, NSW, Australia), were used as starting materials in the present study: Fe_2O_3 (99.98 wt pct purity), NiO (99.99 wt pct purity), MgO (99.99 wt pct purity), Al_2O_3 (99.99 wt pct purity), Fe (99.99 wt pct purity), and Ni (99.8 wt pct purity). The samples were prepared by thoroughly mixing the powders of oxide or combinations of oxide and metal in an agate mortar. The compositions were selected such that two or three condensed phases would be present in the samples after equilibration. The mixtures were then

Table I. Compositions of Phases Observed in the System Fe-Mg-O in Air

				Composition (Metal-Mole Fraction)	
Experiment	Temperature (°C)	Equilibration Time (Hours)	Phases Present	Fe/(Fe + Mg)	Mg/(Fe + Mg)
spinel + periclase					
M-1a	1200	72	spinel	0.648	0.352
			periclase	0.059	0.941
M-6a	1300	72	spinel	0.649	0.350
			periclase	0.128	0.872
M-11	1400	72	spinel	0.670	0.329
			periclase	0.235	0.765
M-27	1500	72	spinel	0.683	0.317
			periclase	0.326	0.674
M-31	1600	72	spinel	0.701	0.299
			periclase	0.393	0.607
hematite + spinel					
M-4a	1200	72	spinel	0.784	0.216
			hematite	0.998	0.002
M-9a	1300	72	spinel	0.890	0.110
			hematite	0.999	0.001

pelletized in a steel die at approximately 40 MPa, to form disks 6 to 10 mm in diameter and 2 mm in thickness. The pellets were fractured to 2 mm in size and the fragments were used for the experiments.

C. *Phase equilibration*

Gas/oxide equilibrations in air atmosphere were carried out in a vertical tube (alumina ceramic with an inner diameter of 32 mm) SiC resistance furnace. A few fragments were placed in a small Pt crucible/basket suspended to a hooked Pt wire placed inside a smaller fixed-alumina tube (inner diameter of 3 mm) in the hot zone of the furnace. The fragments were equilibrated at predetermined temperatures for a certain period of time before the Pt wire was pulled up to unhook the Pt basket, allowing the fragments to fall into the quenching medium located below the furnace. The quenching process occurs in a period of approximately 1 second.

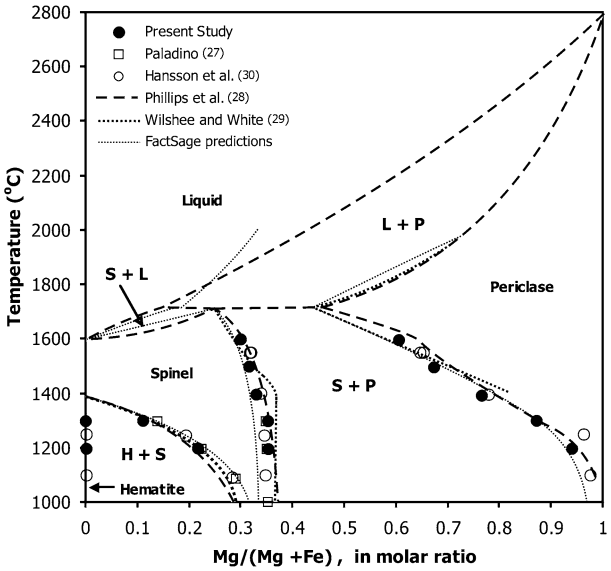

Fig. 1—Pseudobinary phase diagram of 'Fe_2O_3'-MgO in air. Closed-circle data points are results from the present study; light-dotted curves are phase boundaries determined by FactSage. Legend: S = spinel, P = periclase, L = liquid, and H = hematite.

D. *Control of temperature*

The temperature inside the furnace was controlled within ±1 °C. The tip of a calibrated working thermocouple was positioned immediately adjacent to the sample, to track the sample's actual temperature. The working thermocouple was calibrated against a standard thermocouple supplied by the National Measurement Laboratory (CSIRO, Melbourne, Australia). An overall absolute temperature accuracy of ±3 °C is achieved.

E. *Ensuring the achievement of equilibria*

The achievement of an equilibrium state in the samples was ensured by: (1) conducting repeat experiments at extended equilibration times, *i.e.*, doubling or tripling the equilibration time and (2) carrying out selected experiments with the equilibrium compositions approached from two opposite directions, *i.e.*, from more oxidized and more reduced mixture compositions. For example, in the case of the spinel and bunsenite (NiO) equilibrium, the starting compositions of a mixture of Fe_2O_3/NiO powders (with Fe/[Fe + Ni] = 0.5 in moles) and a mixture of FeO/NiO powders (1:1 Fe_2O_3:Fe/NiO with Fe/[Fe + Ni] = 0.5 in moles) were used.

These methods were applied to selected experiments (the experimental data with the diamond symbol, shown in Tables III through V). The achievement of equilibrium in the rest of the experiments was confirmed using only the first method.

The procedure of the equilibration of the samples, similar to the procedure reported previously,[5] is described as follows.

(a) Mixed powder is pelletized then fractured to fragments 2 mm in size.
(b) The fragments are equilibrated at temperature, at set conditions.
(c) A small piece of the sample is mounted and polished and phase compositions are measured using EPMA.
(d) If EPMA results show differences in phase compositions between samples approaching from different

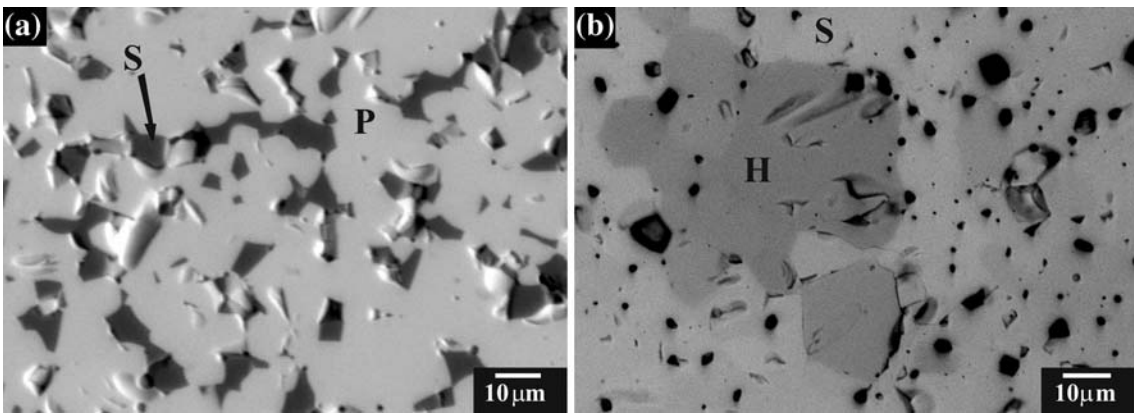

Fig. 2—Examples of microstructure (in backscattered electron mode) observed in Fe-Mg-O system in air at: (*a*) spinel-periclase equilibrium at 1300 °C and (*b*) hematite-spinel equilibrium at 1300 °C. Legend: S = spinel, P = periclase, and H = hematite.

Table II. Compositions of Phases Observed in the System Fe-Al-O in Air

Experiment	Temperature (°C)	Equilibration Time (Hours)	Phases Present	Composition (Metal-Mole Fraction) Fe/(Fe + Al)	Al/(Fe + Al)
hematite + corundum					
A-9	1200	168	corundum	0.104	0.895
			hematite	0.813	0.185
hematite + $Al_2Fe_2O_6$					
A-20	1300	168	hematite	0.797	0.203
			$Al_2Fe_2O_6$	0.519	0.480
spinel + $Al_2Fe_2O_6$					
A-31	1400	72	spinel	0.733	0.267
			$Al_2Fe_2O_6$	0.454	0.546
corundum + $Al_2Fe_2O_6$					
A-19	1300	168	corundum	0.113	0.886
			$Al_2Fe_2O_6$	0.509	0.489
A-32	1400	72	corundum	0.127	0.873
			$Al_2Fe_2O_6$	0.435	0.565

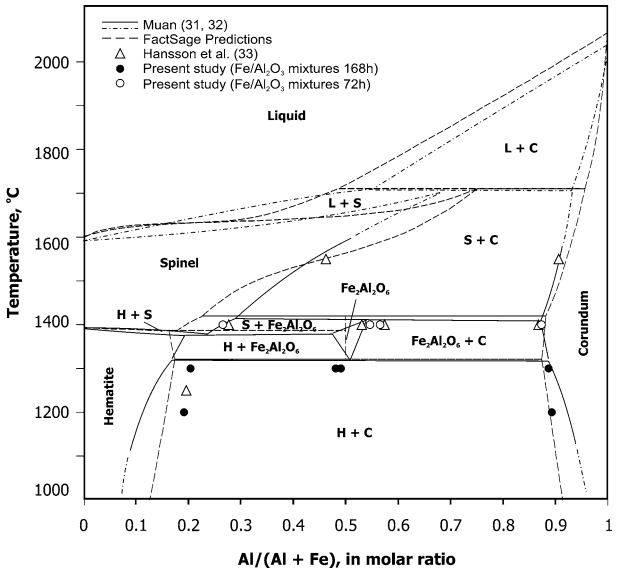

Fig. 3—Pseudobinary phase diagram of 'Fe_2O_3'-Al_2O_3 in air. Closed-circle data points are results from the present study; dashed curves are phase boundaries predicted by FactSage. Legend: S = spinel, L = liquid, C = corundum, and H = hematite.

directions, the samples are then recrushed, pelletized, and equilibrated once more at set conditions.

(e) Steps (b) through (d) are repeated until the compositions of phases in samples approaching equilibria from opposite directions coincided.

F. *Analysis Techniques*

Following the quenching, the samples were dried and then crushed into smaller pieces, to be mounted in epoxy resin and cured in a vacuum chamber. Cross sections of the samples were then prepared by polishing the surface with SiC paper and diamond paste. The sample microstructures were then initially examined using an optical as well as a scanning electron microscope and energy-dispersive X-ray spectroscopy analysis, using a JEOL* 6460LA.

*JEOL is a trademark of Japan Electron Optics Ltd., Tokyo.

An electron probe X-ray microanalyzer, a superprobe JEOL 8200L equipped with five wavelength-dispersive X-ray detectors, was then used to determine the phase compositions of the equilibrated samples. The microanalyzer was operated at 15-kV accelerating voltage and a probe current of 15 nA. The Fe_2O_3, MgO, Al_2O_3 (from the Charles M. Taylor Co., Stanford, CA), and NiO (prepared in-house using NiO, 99.99 wt pct purity) standards were used for the iron, nickel, magnesium, and aluminum calibrations for the EPMA measurements. The Duncumb–Philibert atomic number, absorption, and fluorescence correction procedure supplied with the superprobe JEOL-8200L was applied. The average accuracy of the EPMA measurements was within 1 wt pct.

G. *Phase Equilibria Predictions*

Predictions of the phases and their compositions and proportions formed under equilibrium conditions in the samples were carried out using the FactSage[37] (CRCT, Montreal, Canada and GTT, Aachen, Germany) thermodynamic software (Version 5.5). The appropriate optimized thermodynamic solution databases[38] were used in the modeling; these include solution databases for spinel $(Fe^{2+}, Ni^{2+}, Mg^{2+})[Fe^{3+}, Al^{3+}]_2O_4$, monoxide (wustite and bunsenite) (Fe, Mg, Ni) O_y, and hematite (corundum) $(Fe, Al)_2O_3$.

III. RESULTS AND DISCUSSION

A. *Pseudobinary Phase Diagrams of the 'Fe_2O_3'-MgO, 'Fe_2O_3'-Al_2O_3, and NiO-Al_2O_3 Systems in Air*

Experiments have been carried out on the Fe-Mg-O phase equilibrium in air at temperatures between

Table III. Compositions of Phases Observed in the System Ni-Al-O in Air

Experiment	Temperature (°C)	Equilibration Time (Hours)	Phases Present	Composition (Metal-Mole Fraction) Ni/(Ni + Al)	Al/(Ni + Al)
monoxide + spinel					
A-1♦	1200	168	spinel	0.332	0.668
			bunsenite	0.991	0.009
A-1*♦	1200	72	spinel	0.330	0.670
			bunsenite	0.992	0.008
A-11	1300	168	spinel	0.336	0.664
			bunsenite	0.988	0.012
A-21	1400	168	spinel	0.332	0.667
			bunsenite	0.982	0.018
corundum + spinel					
A-5	1200	168	corundum	0.007	0.993
			spinel	0.305	0.695
A-15	1300	168	corundum	0.008	0.992
			spinel	0.299	0.701
A-25	1400	168	corundum	0.009	0.991
			spinel	0.280	0.718

*Experiments with NiO/Al_2O_3 mixtures as starting materials. The remaining uses Ni/Al_2O_3 mixtures as starting materials.
♦The achievement of equilibrium is confirmed by both extended equilibration times and equilibrations from two opposite directions.

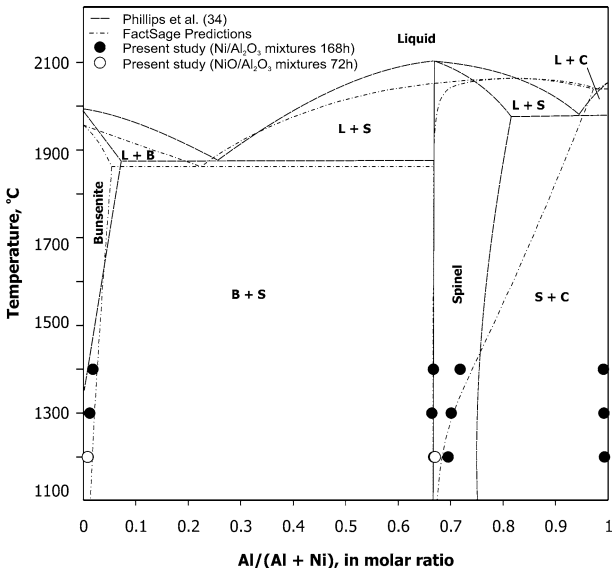

Fig. 4—Pseudobinary phase diagram of $NiO-Al_2O_3$ in air. Closed- and open-circle data points are results from the present study; dashed-dotted curves are phase boundaries predicted by FactSage. Legend: S = spinel, L = liquid, C = corundum, and B = bunsenite.

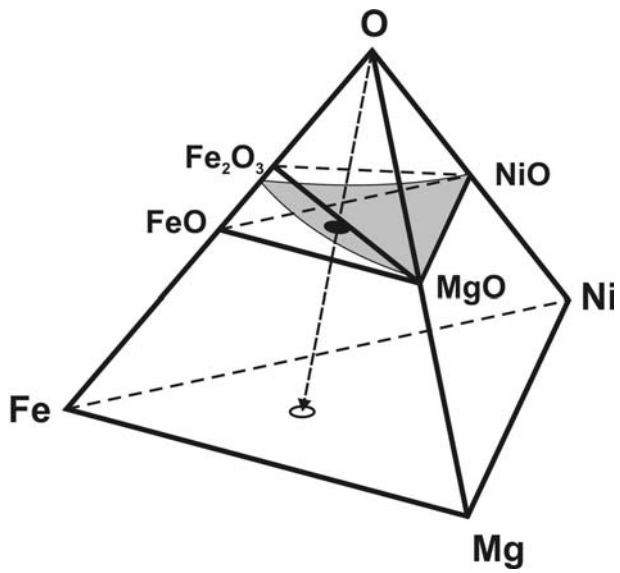

Fig. 5—Schematic of quaternary Fe-Ni-Mg-O system at a fixed temperature. A projection of a composition in $FeO-MgO-NiO-Fe_2O_3$ subsystem onto the Fe-Mg-Ni plane is shown.

1200 °C and 1600 °C, to complement the experiments carried out by Hansson *et al.*[30] The compositions (expressed in metal-mole fractions) measured in the phases at hematite-spinel and spinel-periclase equilibria are reported in Table I. These data were also presented on a pseudobinary 'Fe_2O_3'-MgO phase diagram shown in Figure 1, *i.e.*, closed-circle data points. Previous results by Paladino,[27] Phillips *et al.*,[28] Wilshee and White,[29] and Hansson *et al.*[30] and predictions using FactSage thermodynamic software[37] are also shown in the figure.

The concentration of iron in the spinel phase in equilibrium with hematite increases with increasing temperature; this is in agreement with previous studies. The spinel composition at the spinel/periclase boundary obtained from the current study is also in agreement with previous work by Paladino[27] and Hansson *et al.*[30] The FactSage prediction[37,38] underestimates the Fe concentration of this spinel boundary. The abnormal inflection in the spinel composition at the spinel/periclase boundary at approximately 1400 °C reported by Wilshee and White[29] was not observed in

Table IV. Compositions of Phases Observed in the System Fe-Ni-Mg-O in Air

Experiment	Temperature (°C)	Equilibration Time (Hours)	Phases Present	Composition (Metal-Mole Fraction) Ni/(Ni + Fe + Mg)	Fe/(Ni + Fe + Mg)	Mg/(Ni + Fe + Mg)
hematite + spinel						
M-4	1200	72	spinel	0.057	0.791	0.151
			hematite	0.001	0.998	0.001
M-4a	1200	72	spinel	0	0.784	0.216
			hematite	0	0.998	0.002
M-5	1200	72	spinel	0.157	0.795	0.048
			hematite	0.003	0.996	0.001
EQ-89/103	1200	72	spinel	0.193	0.807	0
			hematite	0.003	0.997	0
M-9	1300	72	spinel	0.032	0.884	0.084
			hematite	0	0.999	0.001
M-9a	1300	72	spinel	0.001	0.889	0.110
			hematite	0	0.999	0.001
M-10	1300	72	spinel	0.082	0.893	0.025
			hematite	0.001	0.998	0
M-10a	1300	72	spinel	0.110	0.890	0
			hematite	0.002	0.998	0
M-20	1300	168	spinel	0.001	0.894	0.105
			hematite	0	0.999	0.001
M-21	1300	168	spinel	0.053	0.903	0.044
			hematite	0.001	0.999	0.001
M-22	1300	168	spinel	0.098	0.902	0.001
			hematite	0.001	0.999	0
spinel + monoxide						
M-1◆	1200	72	spinel	0.078	0.644	0.278
			monoxide	0.207	0.079	0.714
M-1a	1200	72	spinel	0	0.648	0.352
			monoxide	0	0.059	0.941
M-2	1200	72	spinel	0.185	0.660	0.156
			monoxide	0.451	0.119	0.430
M-3◆	1200	72	spinel	0.285	0.658	0.057
			monoxide	0.667	0.162	0.171
EQ-54	1200	168	spinel	0.331	0.669	0
			monoxide	0.839	0.161	0
M-16◆	1200	168	spinel	0.287	0.657	0.056
			monoxide	0.661	0.164	0.174
M-18◆	1200	168	spinel	0.073	0.655	0.272
			monoxide	0.220	0.086	0.694
M-19*◆	1200	168	spinel	0.090	0.655	0.255
			monoxide	0.238	0.077	0.685
M-23◆	1300	168	spinel	0.070	0.663	0.266
			monoxide	0.191	0.155	0.653
M-6◆	1300	72	spinel	0.072	0.652	0.276
			monoxide	0.187	0.149	0.663
M-6a	1300	72	spinel	0	0.649	0.350
			monoxide	0.001	0.128	0.871
M-7	1300	72	spinel	0.179	0.665	0.155
			monoxide	0.424	0.191	0.385
M-8	1300	72	spinel	0.276	0.666	0.057
			monoxide	0.625	0.224	0.151
M-8a	1300	72	spinel	0.334	0.666	0
			monoxide	0.771	0.229	0
M-11	1400	72	spinel	0.0	0.670	0.329
			monoxide	0.0	0.235	0.765
M-12	1400	72	spinel	0.067	0.669	0.264
			monoxide	0.167	0.242	0.590
M-13	1400	72	spinel	0.169	0.666	0.165
			monoxide	0.378	0.256	0.366
M-14	1400	72	spinel	0.268	0.669	0.630
			monoxide	0.578	0.276	0.146

Table IV. Continued

Experiment	Temperature (°C)	Equilibration Time (Hours)	Phases Present	Composition (Metal-Mole Fraction)		
				Ni/(Ni + Fe + Mg)	Fe/(Ni + Fe + Mg)	Mg/(Ni + Fe + Mg)
M-15	1400	72	spinel	0.327	0.673	0
			monoxide	0.715	0.285	0
M-28	1500	72	Spinel	0.097	0.690	0.213
			monoxide	0.218	0.351	0.431
M-29	1500	72	spinel	0.190	0.695	0.115
			monoxide	0.412	0.348	0.240
M-30	1500	72	spinel	0.300	0.699	0
			monoxide	0.636	0.364	0
M-32	1600	72	spinel	0.070	0.704	0.226
			monoxide	0.156	0.401	0.444
M-33	1600	72	spinel	0.146	0.716	0.138
			monoxide	0.309	0.430	0.261
M-34	1600	72	spinel	0.262	0.738	0
			monoxide	0.493	0.506	0

*Experiments with Fe/Ni/MgO mixtures as starting materials. The remaining uses Fe_2O_3/NiO/MgO mixtures as starting materials.
♦The achievement of equilibrium is confirmed by both extended equilibration times and equilibrations from two opposite directions.

the current study; this supports the observation by Hansson *et al.*[30]

The limiting composition of the periclase in equilibrium with the spinel phase in air contains increasing concentrations of iron with increasing temperature. The results from the current study are in agreement with the periclase boundary determined by Wilshee and White[29] and calculated using FactSage. A sharp increase in the solubility of iron in periclase was observed above 1200 °C.

A detailed study of the morphology of the phases formed in the equilibrated samples is beyond the scope of the present article. However, since the quantification of the compositions of phases at a microscopic level is one of the techniques used in the present study, the typical microstructures observed in the samples are presented in the present article. Figures 2(a) and (b) show examples of the microstructure observed in the samples in the case of the spinel-periclase and spinel-hematite equilibria, respectively, at 1300 °C. Different levels of grayscale represent the different phases present in the sample. The phase grains are dense and have a polygon shape, a typical sintered structure (Figure 2). In general, the microstructures equilibrated at higher temperatures were denser (fewer pores and voids) compared to those equilibrated at lower temperatures. No other significant changes in the microstructures were observed with increasing temperature, in the range of conditions studied.

The results of experiments on the Fe-Al-O system in air at temperatures between 1200 °C and 1400 °C carried out in the present study are tabulated in Table II and are also shown in a pseudobinary phase diagram of 'Fe_2O_3'-Al_2O_3 in Figure 3 (closed-circle data points). The results from the Hansson *et al.*[33] open-triangle data points, from Muan,[31,32] and from the FactSage predictions are also shown in the figure.

It can be seen from Figure 3 that, at a temperature of 1200 °C, only hematite and corundum phases were observed. The solubilities of aluminum in the hematite phase and of iron in the corundum phase increase with increasing temperature. The solubility of aluminum in the hematite phase was found to be much higher than the solubilities reported by Muan[31,32] and predicted by FactSage. The present results, however, show the same trend as the results from Hansson *et al.*[33] The iron solubility in corundum at 1200 °C was also found to be higher than that reported by Muan, but is in good agreement with the FactSage predictions.

At 1300 °C, hematite, corundum, and $Fe_2Al_2O_6$ phases were observed. In the previous study by Muan, a $Fe_2Al_2O_6$ phase was reported to form at 1318 °C. It appears that the actual $Fe_2Al_2O_6$ phase field in Figure 3 is bigger than that reported by Muan; it extended down to 1300 °C (note that equilibrium at 1300 °C was approached from a low temperature, starting from pure Fe_2O_3 and Al_2O_3 powders).

Spinel, $Fe_2Al_2O_6$, and corundum phases were observed at a temperature of 1400 °C. The compositions of the spinel (26.7 Al metal-mole pct) and corundum (87.3 Al metal-mole pct) phases at 1400 °C obtained in the present studies are in good agreement with the results from previous studies.[33] The composition range in which the $Fe_2Al_2O_6$ phase is observed, however, was found to be different, compared to the results from Muan. In the present study, the $Fe_2Al_2O_6$ phase was observed in the composition range between 54.6 and 56.5 Al metal-mole pct.

Table III shows the results of experimental studies on the phase equilibria of the Ni-Al-O system in air at temperatures between 1200 °C and 1400 °C. Spinel, bunsenite, and corundum phases were observed in this temperature range. Figure 4 shows the binary phase diagram of NiO-Al_2O_3 in air. The open- and closed-circle data points represent the present results from experiments in which equilibrium was approached from different directions; the same results confirm that the equilibrium state had been attained. The dashed and dashed-dotted curves in Figure 4 are phase boundaries reported by Phillips *et al.*[34] and predicted by FactSage, respectively.

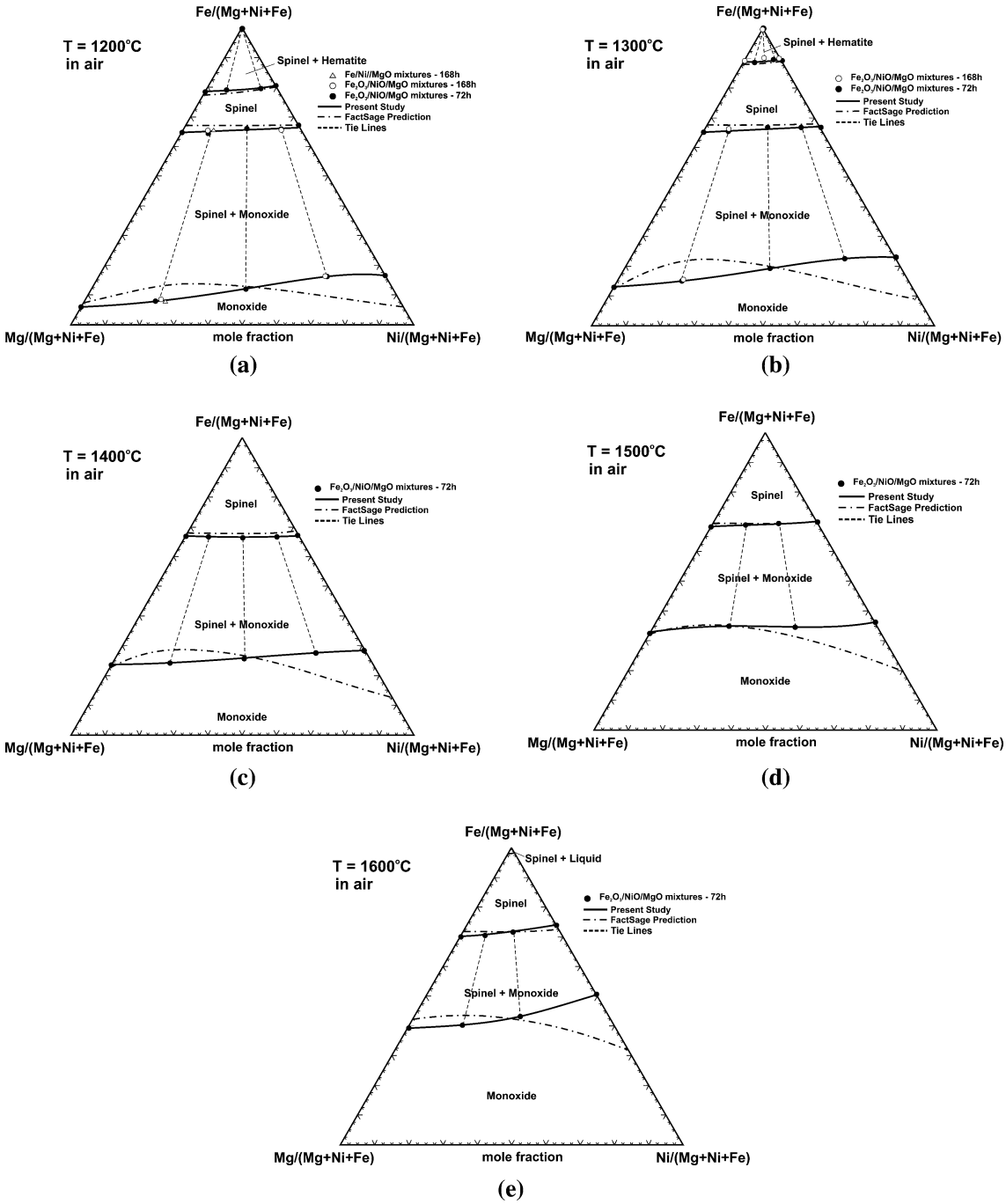

Fig. 6—Ternary Fe-Ni-Mg-O sections in air at: (*a*) 1200 °C, (*b*) 1300 °C, (*c*) 1400 °C, (*d*) 1500 °C, and (*e*) 1600 °C. Solid curves are from the present study, dashed-dotted curves are FactSage predictions, and dashed lines are tie-lines. Legend: S = spinel and M = monoxide.

In the temperature range studied, the solubility of the aluminum in the bunsenite phase does not change significantly with increasing temperature. The aluminum solubility in the bunsenite phase was found to be slightly higher than that reported by Phillips *et al.*[34]

The solubility of aluminum in the spinel phase was observed to increase with increasing temperature and was in a good agreement with the FactSage predictions at 1200 °C and 1300 °C. Above 1400 °C, however, FactSage overestimates the aluminum solubility in the spinel phase. Phillips *et al.*[34] reported a higher aluminum solubility in spinel in this temperature range, *e.g.*, for a composition of spinel 75 Al metal-mole pct at 1400 °C. In the present study, at 1400 °C, the composition of spinel in the spinel + corundum phase field is found to be 71.8 Al metal-mole pct, as shown in Figure 4.

From Figures 1, 3, and 4, it can be seen that there are discrepancies between the results obtained in the present

study and in previous studies.[27–29,31,32,34] The earlier studies were carried out using high-temperature equilibration and quenching techniques followed by XRD, for phase identification and for the determination of phase boundaries. There are several advantages of the EPMA over the XRD technique; these include the following.

(a) Increased accuracy: EPMA, including the measurement of phase composition, is carried out after the equilibration experiment, avoiding uncertainty due to the unavoidable loss of components or materials during the sample preparation and equilibration process, *i.e.*, loss through vapor phase reactions or reactions with materials from the suspender.
(b) Microanalysis capability: The quantitative analysis of the composition of the phases can be carried out accurately in a small area 1 to 2 μm in lateral size, which can be used for evaluating local equilibrium.
(c) Imaging capability: The secondary and backscattered electron imaging provide additional information for evaluating the phases present and their morphology and for evaluating other microstructural characteristics.
(d) Analysis of noncrystalline phases: EPMA can be used to determine the composition of amorphous or glassy phases.

Unlike the EPMA technique, the XRD technique is insensitive to small variations in the concentrations of metal cations for determining the phase boundaries, when there are atoms of similar size in a specific crystallographic position.

Particular equilibration procedures, including extended equilibration times and equilibration from different directions (*i.e.*, from reducing and oxidizing states) and the use of small fragments of materials also ensure the achievement of equilibrium in the present study.

These results for the low-order systems described here are important for characterization of higher-order systems and highlight the differences between the results from the present and previous studies.

B. *Ternary Phase Diagram of the Fe-Ni-Mg-O System in Air*

The Fe-Ni-Mg-O phase equilibria in air at temperatures between 1200 °C and 1600 °C were investigated. In this system, iron can be present in both the ferric and ferrous forms. In the current study, determination of the concentrations of ferric and ferrous irons was not carried out. The phase equilibria data in this system were projected onto the Fe-Mg-Ni plane using the metal atom ratio (schematic in Figure 5).

The compositions of the equilibrium phases determined by EPMA are presented in Table IV and are also plotted in Figures 6(a) through (e).

The tie-lines and phase boundaries from the current study and the phase boundaries predicted by FactSage are also shown in Figure 6. Several trends can be identified from Figure 6. Monoxide, spinel, and hematite were observed at 1200 °C and 1300 °C, and the composition range of the spinel + hematite phase field decreases with increasing temperature (Figures 6(a) and (b)). Between 1400 °C and 1600 °C (Figures 6(c) and (d)), only spinel and monoxide phases were observed in the system. The composition range of the monoxide phase field, in general, expands with increasing temperature between 1200 °C and 1600 °C; that is, the solubility of iron in the monoxide increases with increasing temperature.

Slight discrepancies were observed on the spinel phase boundaries and in the (spinel + monoxide) and (spinel + hematite) phase assemblages between the present results and the FactSage predictions. In contrast, the monoxide-limiting compositions in equilibrium with spinel were found to be significantly different from the FactSage predictions. The FactSage calculations underestimate the maximum solubility of iron in the Ni-rich monoxide phase and overestimate the iron solubility in the Mg-rich monoxide (a Mg/Ni ratio of between 0 and 1).

Typical microstructures observed in the samples in the case of the spinel-hematite equilibrium at 1200 °C and the spinel-monoxide equilibrium at 1400 °C are shown in Figures 7(a) and (b), respectively. Dense polygon-shaped phases and grains were observed in these samples. No significant changes in the microstructure between 1200 °C and 1600 °C were observed.

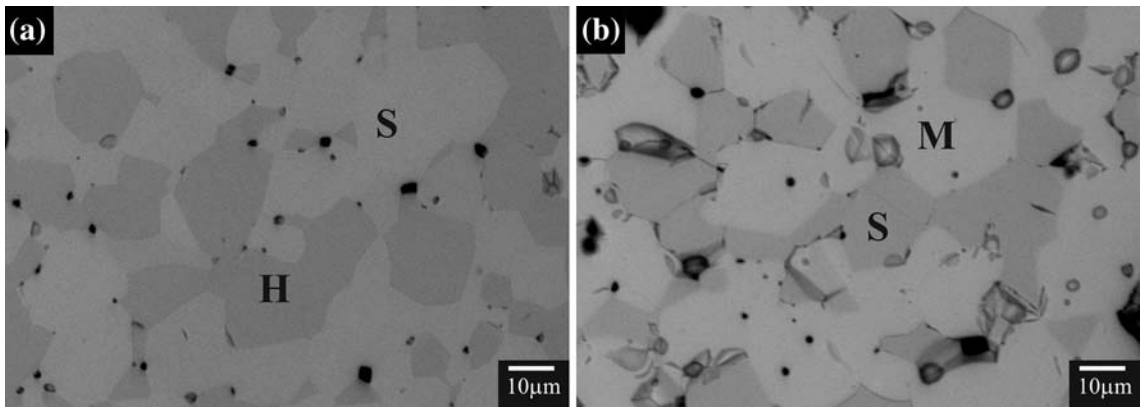

Fig. 7—Examples of microstructure (in backscattered electron image) observed in the Fe-Ni-Mg-O system in air: (*a*) spinel-hematite equilibrium at 1200 °C and (*b*) spinel-monoxide equilibrium at 1400 °C. Legend: S = spinel, H = hematite, M = monoxide, and black area = pores.

Table V. Compositions of Phases Observed in the System Fe-Ni-Al-O in Air

Experiment	Temperature (°C)	Equilibration Time (Days)	Phases Present	Composition (Metal-Mole Fraction) Ni/(Ni + Fe + Al)	Fe/(Ni + Fe + Al)	Al/(Ni + Fe + Al)
monoxide + spinel						
A-1◆	1200	168	spinel	0.332	0	0.668
			monoxide	0.991	0	0.009
A-1*◆	1200	72	spinel	0.330	0	0.670
			monoxide	0.992	0	0.008
A-2	1200	168	spinel	0.327	0.203	0.470
			monoxide	0.897	0.085	0.018
A-3	1200	168	spinel	0.331	0.503	0.166
			monoxide	0.832	0.154	0.014
A-4	1200	168	spinel	0.326	0.674	0
			monoxide	0.829	0.171	0
A-11	1300	168	spinel	0.336	0	0.664
			monoxide	0.988	0	0.012
A-12◆	1300	168	spinel	0.334	0.235	0.431
			monoxide	0.865	0.107	0.028
A-12*◆	1300	72	spinel	0.326	0.229	0.445
			monoxide	0.878	0.097	0.025
A-13	1300	168	spinel	0.336	0.509	0.155
			monoxide	0.789	0.192	0.019
A-14	1300	168	spinel	0.332	0.668	0
			monoxide	0.774	0.226	0
A-21	1400	168	spinel	0.332	0	0.667
			monoxide	0.982	0	0.018
A-22◆	1400	168	spinel	0.324	0.237	0.439
			monoxide	0.829	0.133	0.038
A-22*◆	1400	72	spinel	0.327	0.228	0.445
			monoxide	0.835	0.125	0.040
A-23	1400	168	spinel	0.321	0.511	0.168
			monoxide	0.749	0.224	0.027
M-15*	1400	72	spinel	0.327	0.673	0
			monoxide	0.715	0.285	0
corundum + spinel						
A-5	1200	168	corundum	0.007	0	0.993
			spinel	0.305	0	0.695
A-6	1200	168	corundum	0.004	0.005	0.991
			spinel	0.268	0.255	0.478
A-7	1200	168	corundum	0.004	0.016	0.980
			spinel	0.187	0.510	0.303
A-15	1300	168	corundum	0.008	0	0.992
			spinel	0.299	0	0.701
A-16	1300	168	corundum	0.005	0.007	0.988
			spinel	0.239	0.219	0.542
A-17	1300	168	corundum	0.002	0.041	0.956
			spinel	0.159	0.436	0.405
A-25	1400	168	corundum	0.009	0	0.991
			spinel	0.280	0	0.718
A-26	1400	168	corundum	0.006	0.016	0.978
			spinel	0.203	0.178	0.619
A-27	1400	168	corundum	0.003	0.070	0.927
			spinel	0.142	0.378	0.480
A-29	1400	168	corundum	0.001	0.109	0.890
			spinel	0.038	0.639	0.323
A-30	1400	168	corundum	0	0.117	0.883
			spinel	0.025	0.670	0.305
hematite + spinel						
EQ-89/103*	1200	72	hematite	0.003	0.997	0
			spinel	0.193	0.807	0
A-8*	1200	72	hematite	0.003	0.915	0.082
			spinel	0.181	0.696	0.123
M-10a*	1300	72	hematite	0.002	0.998	0
			spinel	0.110	0.890	0

Table V. Continued

Experiment	Temperature (°C)	Equilibration Time (Days)	Phases Present	Composition (Metal-Mole Fraction) Ni/(Ni + Fe + Al)	Fe/(Ni + Fe + Al)	Al/(Ni + Fe + Al)
A-18*	1300	72	hematite	0.007	0.910	0.083
			spinel	0.011	0.784	0.106
corundum + hematite + spinel						
A-9	1200	168	corundum	0.001	0.104	0.895
			hematite	0.002	0.813	0.185
			spinel	0.155	0.561	0.284
corundum + $Al_2Fe_2O_6$ + spinel						
A-19	1300	168	corundum	0.001	0.113	0.886
			$Al_2Fe_2O_6$	0.002	0.509	0.489
			spinel	0.085	0.637	0.277
hematite + $Al_2Fe_2O_6$ + spinel						
A-20	1300	168	hematite	0	0.797	0.203
			$Al_2Fe_2O_6$	0.001	0.519	0.480
			spinel	0.063	0.679	0.258

*Experiments with $Fe_2O_3/NiO/Al_2O_3$ mixtures as starting materials. The remaining uses $Fe/Ni/Al_2O_3$ mixtures as starting materials.
♦The achievement of equilibrium is confirmed by both extended equilibration times and equilibrations from two opposite directions.

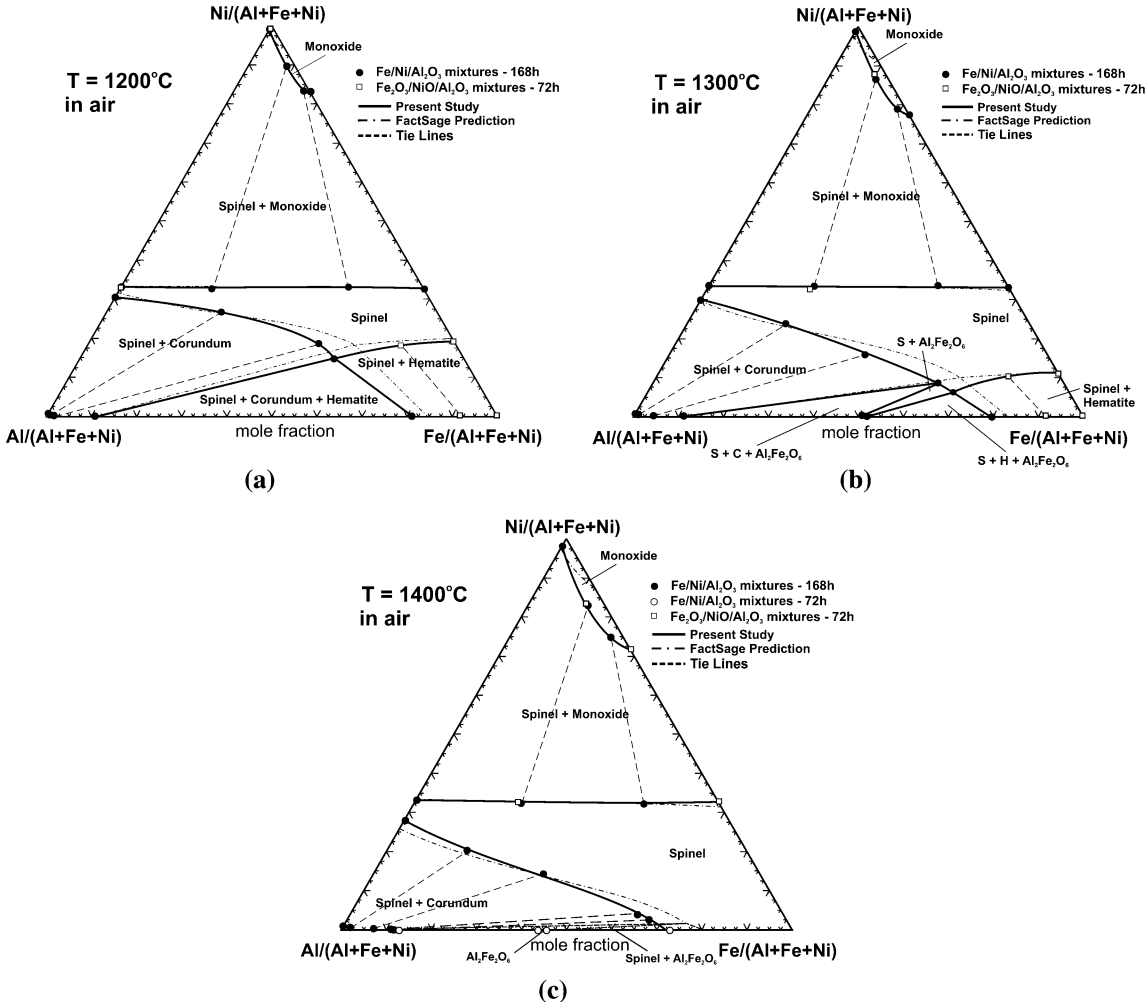

Fig. 8—Ternary Fe-Mg-Al-O sections in air at: (*a*) 1200 °C, (*b*) 1300 °C, and (*c*) 1400 °C. Solid curves are from the present study, dashed-dotted curves are FactSage predictions, and dashed lines are tie-lines. Legend: S = spinel, M = monoxide, and C = corundum.

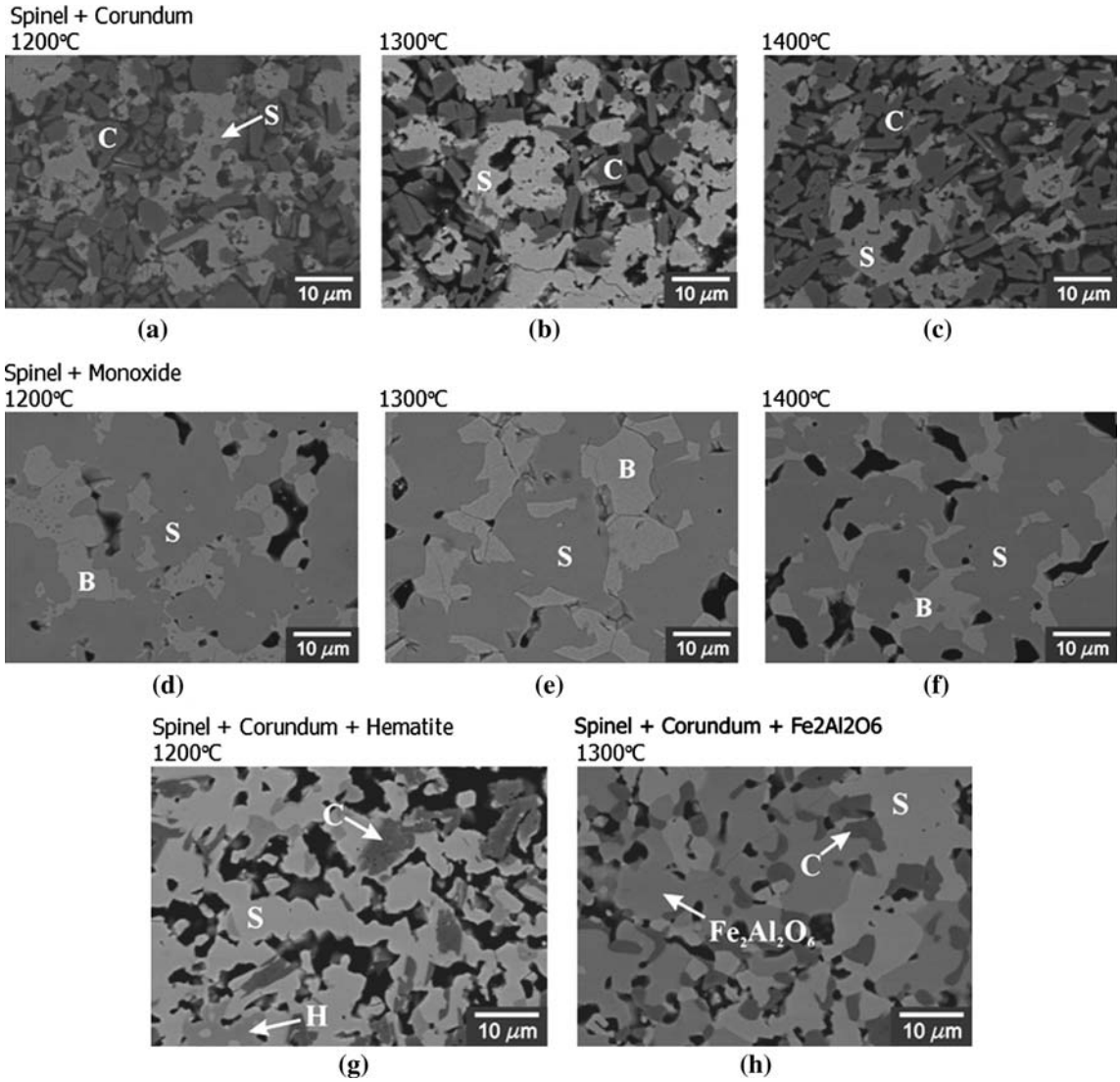

Fig. 9—Examples of microstructure (backscattered electron image) observed in Fe-Ni-Al-O system in air. Spinel-corundum equilibria are shown at (*a*) 1200 °C, (*b*) 1300 °C, and (*c*) 1400 °C; spinel-monoxide equilibria are shown at (*d*) 1200 °C, (*e*) 1300 °C, and (*f*) 1400 °C; (*g*) spinel + corundum + hematite equilibrium is shown at 1200 °C; and (*h*) spinel + corundum + $Fe_2Al_2O_6$ equilibrium is shown at 1300 °C. Legend: S = spinel, C = corundum, H = hematite, and B = bunsenite.

C. *Ternary Phase Diagram of Fe-Ni-Al-O System in Air*

The results of the phase equilibria study of the Fe-Ni-Al-O system in air at temperatures between 1200 °C and 1400 °C are given in Table V. The results are also shown in phase diagrams; similar to the case of the Fe-Ni-Al-O system, the phase equilibria data are projected onto the Fe-Al-Ni plane, as shown in Figures 8(a) through (c). The solid and dashed-dotted curves are phase boundaries obtained from the present study and the FactSage calculations, respectively. The dashed lines are the tie-lines obtained from the present study.

It can be seen from Figure 8 that, in the temperature range studied, the composition range of the monoxide phase field expands with increasing temperature; both the aluminum and the iron solubilities in monoxide increase with increasing temperature. The composition range of the spinel phase field was also observed to expand with increasing temperature. In contrast, the composition range of the spinel + hematite phase field decreases with increasing temperature.

Spinel, corundum, monoxide, and hematite phases were observed at 1200 °C. Spinel, corundum, and hematite can coexist, forming a three-phase equilibrium, as shown in Figure 8(a). At 1300 °C, in addition to the aforementioned phases, $Fe_2Al_2O_6$ was also observed. Two three-phase equilibria of spinel + corundum + $Fe_2Al_2O_6$ and spinel + hematite + $Fe_2Al_2O_6$ assemblages were observed at 1300 °C, as shown in Figure 8(b). Spinel, corundum, monoxide, and $Fe_2Al_2O_6$ were present at 1400 °C. No three-phase equilibria were observed at 1400 °C.

Some discrepancies between the present results and the FactSage predictions (Figure 8) were observed. The FactSage thermodynamic solution databases were

optimized based on the previously available experimental data (*e.g.*, data from lower-order systems). As has been pointed out in Section III–A, these lower-order systems are not fully characterized and the previously available data need to be revised. Therefore, the differences between the results from the present study and the FactSage predictions can be expected.

Figure 9 shows examples of microstructures observed in the Fe-Ni-Al-O system in air at various temperatures. The black areas in these figures are pores. Figures 9(a) through (c) show the microstructures in the samples with spinel-corundum equilibrium. It appears that the corundum phase exhibits a thick platelike morphology, while the spinel exhibits a more equiaxed polygon morphology. There are no significant differences in the microstructure of the samples at 1200 °C, 1300 °C, and 1400 °C. Examples of microstructures in the samples with the spinel-monoxide equilibrium are shown in Figures 9(d) and (f). It can be seen from the figures that both spinel and monoxide phases exhibit polygon morphology. It also appears that there are no significant differences in the microstructure at 1200 °C, 1300 °C, and 1400 °C. Examples of microstructures of the three-phase equilibria spinel-corundum-hematite and spinel-corundum-$Fe_2Al_2O_6$ are shown in Figures 9(g) and (h), respectively. The spinel, hematite, and $Fe_2Al_2O_6$ phases in these microstructures exhibit polygonal morphology. The corundum phase, in the case of the spinel + corundum + hematite phase equilibria, exhibits a platelike morphology (Figure 9(g)); however, in the case of the spinel + corundum + $Fe_2Al_2O_6$, a more rounded morphology is exhibited (Figure 9(h)).

IV. CONCLUSIONS

The phase equilibria of the Fe-Ni-Mg-O and Fe-Ni-Al-O systems, including their lower-order systems, 'Fe_2O_3'-MgO, 'Fe_2O_3'-Al_2O_3, and NiO-Al_2O_3, at temperatures between 1200 °C and 1600 °C in air at the subsolidus region have been experimentally studied. It was found that there are some differences between the present data and the data published previously. It is suggested that the improved experimental techniques used in the present study provide more accurate and precise measurements of the phase boundaries and compositions.

In the case of 'Fe_2O_3'-Al_2O_3 binary phase diagram, the solubilities of aluminum in hematite and of iron in corundum were found to be much larger than those reported in the previous studies. The $Fe_2Al_2O_6$ phase was observed to form at temperatures as low as 1300 °C, in contrast to 1318 °C, as was previously reported. In the case of the NiO-Al_2O_3 binary phase diagram, the present results suggested a lower aluminum solubility in the spinel phase.

In the Fe-Ni-Mg-O system, FactSage calculations underestimate the Fe solubility in the Ni-rich monoxide phase and generally overestimate the Fe solubility in the Mg-rich monoxide (a Mg/Ni ratio of between 0 and 1). In the Fe-Ni-Al-O system, FactSage underestimates the solubilities of Fe and Al in the monoxide phase. Three three-phase equilibria were observed in the system in the temperature range studied, *i.e.*, spinel + corundum + hematite, spinel + corundum + $Fe_2Al_2O_6$, and spinel + hematite + $Fe_2Al_2O_6$.

ACKNOWLEDGMENTS

The authors thank the Australian Research Council and the BHP Billiton Yabulu refinery at Townsville, Australia, for their financial support for this research (Grant No. ARC LP0562201), which was undertaken under the auspices of the Australian Research Council Linkage program.

REFERENCES

1. M.H. Caron: *Trans. AIME*, 1950, vol. 188, pp. 67–90; U.S. Patent 1,346,175, 1920.
2. M.A. Rhamdhani, E. Jak, and P.C. Hayes: *Metall. Mater. Trans. B*, 2008, vol. 39B, pp. 218–33.
3. M.A. Rhamdhani, P.C. Hayes, and E. Jak: *Miner. Process. Extr. Metall. (Trans. Inst. Min. Metall., Sect. C)*, 2009.
4. M.A. Rhamdhani, P.C. Hayes, and E. Jak: *Miner. Process. Extr. Metall. (Trans. Inst. Min. Metall., Sect. C)*, 2009.
5. M.A. Rhamdhani, P.C. Hayes, and E. Jak: *Metall. Mater. Trans. B*, 2008, vol. 39B, pp. 690–701.
6. V. Raghavan: *Phase Diagrams of Ternary Iron Alloys, Part 5. Ternary Systems Containing Iron and Oxygen*, Indian Institute of Metals, Calcutta, India, 1989, pp. 222–31.
7. R. Luoma: *CALPHAD*, 1995, vol. 19 (3), pp. 279–95.
8. G.S. Viktorovich, V.A. Gutin, and D.I. Lisovskii: *Tsvetn. Met. (Moscow)*, 1966, vol. 39 (12), pp. 54–57.
9. G.S. Viktorovich and D.I. Lisovskii: *Tsvetn. Met. (Moscow)*, 1966, vol. 39 (11), pp. 49–55.
10. G.S. Viktorovich, D.I. Lisovskii, and V.A. Gutin: *Russ. J. Phys. Chem.*, 1969, vol. 43 (12), pp. 1709–11.
11. G.S. Viktorovich, R.Y. Dobrovinskii, V.S. Zhagalov, D.I. Lisovskii, A.N. Men, and G.I. Chufarov: *Russ. J. Phys. Chem.*, 1970, vol. 44 (1), pp. 116–18.
12. G.S. Viktorovich, V.S. Zhagalov, and D.I. Lisovskii: *Russ. J. Phys. Chem.*, 1972, vol. 46 (6), pp. 881–82.
13. A.D. Dalvi and R. Sridhar: *Can. Metall. Q.*, 1976, vol. 15 (4), pp. 349–57.
14. G.A. Roeder and W.W. Smeltzer: *J. Electrochem. Soc.*, 1964, vol. 111 (9), pp. 1074–78.
15. H. Davies and W.W. Smeltzer: *J. Electrochem. Soc.*, 1972, vol. 119 (10), pp. 1362–68.
16. A.D. Dalvi and W.W. Smeltzer: *J. Electrochem. Soc.*, 1970, vol. 117 (11), pp. 1431–36.
17. A.D. Dalvi and W.W. Smeltzer: *J. Electrochem. Soc.*, 1974, vol. 121 (3), pp. 386–94.
18. F. Schneider and H. Schmalzried: *Z. Phys. Chem. Neue Folge*, 1990, vol. 166, pp. 1–18.
19. A.E. Paladino, Jr.: *J. Am. Ceram. Soc.*, 1959, vol. 42 (4), pp. 168–75.
20. M.W. Shafer: *J. Phys. Chem.*, 1961, vol. 65, pp. 2055–62.
21. I. Katayama, Y. Watanabe, and Z. Kozuka: *Trans. JIM*, 1979, vol. 20, pp. 593–96.
22. A.D. Pelton, H. Schmalzried, and J. Stitcher: *J. Phys. Chem. Solids*, 1979, vol. 40, pp. 1103–22.
23. P.Y. Eveno and M.P. Paulus: *Proc. 8th Int. Symp. Reactivity of Solids*, Wiley Interscience Publication, New York, NY, 1976, p. 433.
24. H.S. Roberts and H.E. Merwin: *Am. J. Sci.*, 1931, vol. 21 (122), pp. 145–57.
25. R.G. Richards and J. White: *J. Trans. Br. Ceram. Soc.*, 1954, vol. 53, pp. 422–59.
26. D. Woodhouse and J. White: *J. Trans. Br. Ceram. Soc.*, 1955, vol. 54, pp. 333–66.

27. A.E. Paladino, Jr.: *J. Am. Ceram. Soc.*, 1960, vol. 43 (4), pp. 183–91.
28. B. Phillips, S. Somiya, and A. Muan: *J. Am. Ceram. Soc.*, 1961, vol. 44 (4), pp. 167–69.
29. J.C. Wilshee and J. White: *J. Trans. Br. Ceram. Soc.*, 1967, vol. 66, pp. 541–55.
30. R. Hansson, P.C. Hayes, and E. Jak: *Scand. J. Metall.*, 2004, vol. 33, pp. 355–61.
31. A. Muan and C.L. Gee: *J. Am. Ceram. Soc.*, 1956, vol. 39 (6), pp. 207–14.
32. A. Muan: *Am. J. Sci.*, 1958, vol. 256, pp. 413–22.
33. R. Hansson, P.C. Hayes, and E. Jak: *Metall. Mater. Trans. B*, 2004, vol. 35B, pp. 633–42.
34. B. Phillips, J.J. Hutta, and I. Warshaw: *J. Am. Ceram. Soc.*, 1963, vol. 46 (12), pp. 579–83.
35. Y. Iida: *J. Jpn. Soc. Powder Met.*, 1959, vol. 6 (2), pp. 55–58.
36. E. Jak, P.C. Hayes, and H.G. Lee: *Kor. J. Met. Mater.*, 1995, vol. 1, pp. 1–8.
37. C.W. Bale, P. Chartrand, S.A. Degterov, G. Eriksson, K. Hack, R. Ben Mahfoud, J. Melancon, A.D. Pelton, and S. Petersen: *CALPHAD*, 2002, vol. 26, pp. 189–228.
38. S.A. Decterov, I.-H. Jung, E. Jak, Y.-B. Kang, P. Hayes, and A.D. Pelton: *Proc. VIIth Int. Conf. Molten Slags, Fluxes, and Salts, Capetown*, SAIMM, Johannesburg, South Africa, 2004, pp. 839–50.